Available online at www.sciencedirect.com
ScienceDirect
International Journal of Heat and Mass Transfer 50 (2007) 3649–3657
International Journal of HEAT and MASS TRANSFER
www.elsevier.com/locate/ijhmt

Subcooled flow boiling CHF enhancement with porous surface coatings

Mohammad Sohail Sarwar *, Yong Hoon Jeong, Soon Heung Chang

Korea Advanced Institute of Science and Technology 373-1, Guseong-dong, Yuseong-gu, Daejeon 305-701, Republic of Korea

Received 15 May 2006; received in revised form 19 September 2006
Available online 8 December 2006

Abstract

The effect of micro/nanoporous inside surface coated vertical tubes on CHF was determined during water flow boiling at atmospheric pressure. CHF was measured for smooth and three different coated tubes, at mass fluxes (100–300 kg/m^2 s) and two inlet subcooling temperatures (50 °C and 75 °C). Greater CHF enhancement was found with microporous coatings than with nanoporous coatings. Al_2O_3 microporous coatings with particle size <10 μm and coatings thickness of 50 μm showed the best CHF enhancement. Maximum increase in CHF was about 25% for microporous Al_2O_3. A wettability test was performed to study an increase of CHF with microporous coated surfaces.

Keywords: Flow boiling; CHF; Porous coatings; Wettability

1. Introduction

Critical heat flux (CHF) refers to the heat transfer limit causing a sudden rise in surface temperature under heat flux controlled conditions and possible catastrophic failure of a device in which evaporation or boiling is occurring. This condition defines the upper limit of safe operation of heat transfer equipment employing boiling heat transfer in heat flux controlled systems [1]. CHF of forced convective boiling is a phenomenon that has been considered as one of the most important parameters in designing and operating heat transfer equipment with a high heat flux, such as steam generators, evaporator, superconducting magnets, electronic equipment, and rocket engines. In nuclear power plants, insufficient cooling during an overpower transient or a loss of coolant accident may cause CHF leading to core meltdown and subsequent release of radioactive material into the environment.

Metallic or ceramic porous coatings have been evaluated for increasing CHF and many studies have investigated the surface conditions for CHF enhancement [2,3,6–17]. Important geometric parameters in these studies are particle size, particle shape, coating thickness and porosity. Porous coated surfaces act as a boiling enhancement due to increased number of small scale cavities on the surface, resulting in a high particle surface area (high surface to volume ratio) of uniform pore size in the micrometer range. Each void/pore is interconnected and assists the flow of fluid towards the heated surface. CHF enhancement is due to capillary assisted liquid flow towards a phase-change interface. It reduces liquid vapor counter flow resistance and hinders the development of localized dryout conditions. Capillary pumping in porous media generates the required liquid draw, establishing a fluid flow artery [3–5]. The effective boiling surface area is the vapor-liquid contact surface area that exists within pores formed between stacked particles.

The geometry of a cavity containing trapped vapor is directly related to the bubble nucleation process. By manufacturing optimum cavity sizes on a heat surface, nucleate boiling heat transfer can be efficiently increased [6–13,19,20]. Ammerman and You [9] felt that the mechanism of CHF enhancement from a coating is due to an increased number of nucleation sites. Bubble departure frequency

* Corresponding author. Tel.: +82 42 869 3856; fax: +82 42 869 3810.
E-mail addresses: sohail@kaist.ac.kr (M.S. Sarwar), jeongyh@kaist.ac.kr (Y.H. Jeong), shchang@kaist.ac.kr (S.H. Chang).

0017-9310/$ - see front matter © 2006 Elsevier Ltd. All rights reserved.
doi:10.1016/j.ijheatmasstransfer.2006.09.011

Nomenclature

A	ampere	R	resistance (Ω)
A	flow area (m^2)	RMS	root mean square
CHF	critical heat flux (kW/m^2)	t_c	coating thickness (μm)
D	tube diameter (m)	V	volt
d	particle size (μm)		
G	mass flux (kg/m^2 s)	*Greek symbol*	
g	gram	ρ	resistivity (Ω m)
h	heat transfer coefficient (W/m^2 s)		
k	thermal conductivity (W/m K)	*Subscript*	
L	length of a heated tube (m)	c	coating

and surface coatings provides a means for which boiling dominates over convection.

The effect of micro/nanoporous coating on CHF has not been sufficiently investigated under flow boiling conditions. Most research has considered only pool boiling. The effect of surface coatings on CHF during flow boiling needs further study at low mass flow rates and at low pressures.

Chang and You [2,10] used alumina (Al_2O_3), diamond and silver particles (1–70 μm) as the coating material to test in pool boiling experiment with FC-72 (refrigerant) at atmospheric pressure. The particles adhered to the surface due to Van der Walls molecular attraction forces. Significant reduction in incipient and nucleate boiling superheats (~50%) and an increase in CHF (~32%) were reported [2,10]. O'Connor and You [13], using boiling enhancement paint with silver flakes (3–10 μm), showed an 80% reduction in nucleate boiling superheat and a 109% increase in CHF over non-painted surfaces. They performed pool boiling experiment with FC-72 refrigerant at atmospheric pressure. The coating technique used epoxy with micro-size particles and isopropyl alcohol (or methyl-ethyl-ketone, M.E.K.) as carrier [13]. This simple and economical technique produced highly enhanced nucleation with lower incipient superheat and enhanced CHF over an uncoated surface.

Vemuri and Kim [6] performed a pool boiling heat transfer experiment from a nanoporous surface immersed in a saturated FC-72 dielectric fluid at atmospheric pressure (101 kPa). The diameter of the Alumina (Al_2O_3) nanoporous surface ranged from 50 to 250 nm. They compared the results of a nanoporous surface with a plain surface and obtained a decrease of 30% in the incipient superheat for the nanoporous surface. Schroeder-Richter [7] conducted a water flow boiling study with plain and porous tubes at atmospheric pressure. They used low mass flux (0–200 kg/m^2 s) and inlet subcooling temperature of 3–55 K. Tomoaki Kunugi et al. [8] etched the surface with HNO_3 and used 100 nm sized particles made from copper oxide, carbon nanotube and aluminum oxide, reporting an increase of about 180% in the heat transfer coefficient. They observed the heat transfer performance by evaluating a ratio between heat transfer rate at the surface of the top plate and that at the bottom plate.

This study examines water flow boiling CHF enhancement using micro/nanoporous coatings on a half-inch (12.7 mm) circular tube's inner surface. The objective of the study is to investigate CHF enhancement using different porous coatings of alumina (particle size, $d < 10$ μm), alumina ($d < 1$ μm) and TiO_2 ($d < 5$ μm). The experiments were performed at atmospheric pressure, a low mass flux (100–300 kg/m^2 s) and at an inlet subcooling temperature of 50–75 °C. The flow boiling experiment was performed with three different coated tubes under fixed inlet conditions. Results were compared with the reference smooth (un-coated) tube to see the effect of microporous and nanoporous coatings on CHF. In addition, a wettability test was performed to substantiate the evidence of water entrapment in the porous coatings.

2. Experimental apparatus and procedure

2.1. Experimental loop

The flow boiling heat transfer experiment was performed at high heat flux up to CHF at the Korea Advanced Institute of Science and Technology (KAIST). A closed water flow boiling loop with a test section was heated directly using an electrical DC power supply unit. The schematic diagrams of test loop and tubular test section are shown in Figs. 1 and 2. The experiments were carried out at atmospheric pressure by venting to ambient. The main test loop consisted of a condenser, surge tank (with overhead water reservoir), a centrifugal pump, turbine flow meter, two pre-heaters (to control the inlet water temperature and subcooling), needle valve (to provide throttling) and a test section. Thermocouples and pressure transducers were connected to a HP 3852A data acquisition/control unit for data collection and processing.

2.2. Test section

The water flows in an upward direction in the test section tube, which is coated from the inner side. The dimen-

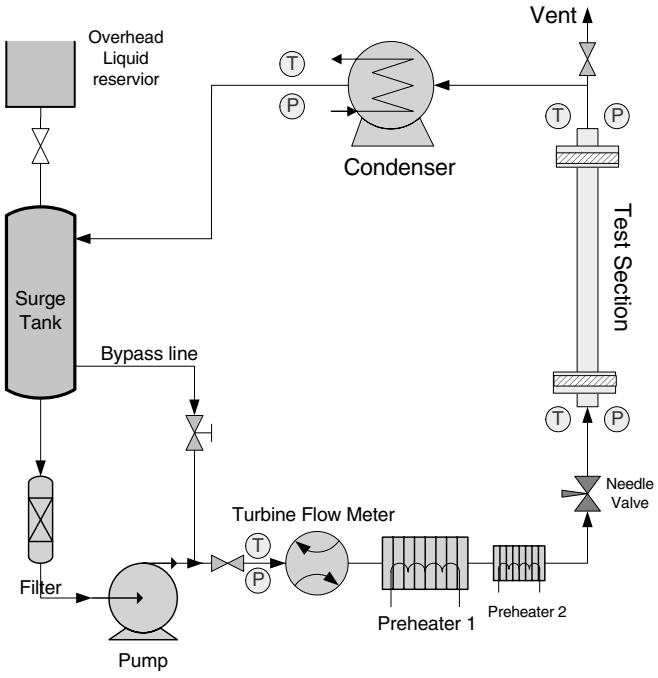

Fig. 1. Schematic diagram of experimental test loop. *T*: Temperature, *P*: Pressure.

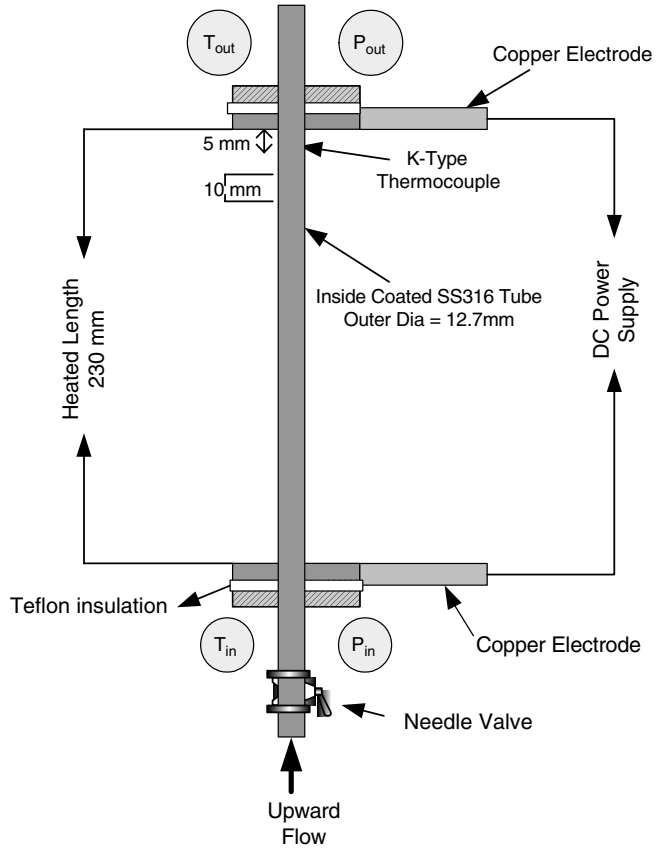

Fig. 2. Schematic diagram of the test section.

sions of the cylindrical tube and flow parameters are listed in Table 1. The test section was made of SS-316 circular tube of outer diameter 12.7 mm and length of 230 mm. Three Type-K thermocouples (outer diameter = 1.5 mm) were attached onto the outer surface of the test section to detect wall temperature. The first thermocouple was located at 5 mm below the end of the upper power clamp. The distance between each thermocouple was 10 mm. Copper electrodes were provided to connect the heated length of tube with the DC power supply which controlled the power by power transformer with a maximum capacity of 32 V and 2000 A, heated by Joule heating. The test section was connected to the flange, which was insulated from rest of the part of the test loop by Teflon. The current and voltage difference between both ends of the test section were measured and collected by data acquisition system. The temperatures of the water at the inlet and outlet of the test section were measured with in-stream T-type sheathed thermocouples. Outlet pressure and inlet pressure were measured with pressure transducers and calibrated to 0.5% of RMS error for a full range.

Table 1
Test matrix

	Parameters	
Uniformly heated vertical cylindrical tube		
Geometry	Outer diameter	12.7 mm
	Inner diameter	10.92 mm
	Heated length	230 mm
Vertical upward flow		
Flow	Pressure	101.3 kPa (1 atm.)
	Mass flux	100–300 kg/m^2 sec
	Inlet subcooling	50–75 °C

2.3. Test procedure and test matrix

CHF data was taken for all test conditions. The experimental loop was filled with filtered water, which was heated in the loop by preheaters in order to remove non-condensable gas. Degassing was conducted at atmospheric pressure, with opening of vent valves on top of the surge tank and preheaters, and stopped when gas was not detected in the venting line. Heat balance tests performed before each series of experiments showed heat losses to be <2%. Entering water temperature in the test section was kept constant by electronically controlled preheaters in series. Flow rate was measured by a turbine flow meter (Omega FTB 505 VDC, 0.2–2.0 gallon/min), and mass flux was calculated in real time.

During the measurements, the heating power in the test section was gradually increased by slowly increasing the voltage. The heat flux increment used near the CHF was ~10 kW/m^2. The voltage of the test section increased step by step with enough duration for the thermal equilibrium of the water and stabilization of temperature detection. At least two consecutive runs were conducted for each surface tested. CHF condition was defined as a sudden increase in the temperature (~50 °C) of the tube surface

and CHF onset position was considered as a point where the first temperature jump takes place. CHF was assumed to occur when the wall temperature showed sudden increase with the slight increase of heat flux. At that moment, power to the test section was immediately switched off to avoid damage to the heated surface. Heat flux was calculated from applied voltage and resistance in the heating element. CHF experiments were performed at two different inlet subcooling temperatures (50 °C and 75 °C) and three different mass flux levels (100, 200 and 300 kg/m^2 s), (Table 1).

2.4. Experimental uncertainty analysis

Uncertainty analyses were estimated by the method of Moffat [18]. Mass flux uncertainty was estimated as 5% at 100 and 200 kg/m^2 s and 3.5% at 300 kg/m^2 s. Uncertainty in pressure measurements were estimated as 3%. To avoid any measurement variation error between the three test section thermocouples, a test run was performed for each heater. The temperature measurement uncertainties were primarily estimated considering the thermocouple calibration and temperature correction from the thermocouple reading to the reference surface. The maximum variation of three measured wall temperatures (K-type thermocouples) was ±0.5 °C. The uncertainty in the inlet and outlet water temperatures (T-type thermocouples) was estimated to be less than ±1 °C. The maximum error in controlling inlet subcooling temperature, by the help of two preheaters, was ±2 °C.

Uncertainty in heat flux was observed by taking into account the voltage and electrical resistance ($R = \rho\frac{L}{A}$) uncertainties, where ρ is resistivity and L and A are length and flow area, respectively. To estimate heat losses to external surroundings, conservative calculations performed at various heat flux conditions for the heated test section geometry. Heat losses were calculated at different heat flux conditions with the help of computer code (FLUENT 6.0). Heat losses to the surroundings were less than 1.0% for heat flux conditions of 100–900 kW/m^2, assuming the uniform temperature distribution with heater surface temperature of 180 °C. Heated surface area also contributed in the uncertainty. Considering all these factors, the overall uncertainty in heat flux was ~4% while taking in to account the uncertainties of heat flux and power, the uncertainty in the CHF was around 5%.

During wettability test, smooth and coated tubes were weighed dry, soaked in water and re-weighed three times to know the error in measurements. The digital weighing balance Ohaus Scout II was used for recording measurements and RMS error of 1.5% was observed in measurements, while the linearity of weighing scale was ±0.01 g.

3. Coating composition and process

A high nucleation site density and optimized cavity structure are required for boiling heat transfer and CHF enhancement. The technique of O'Connor and You was used to produce porous coating structure inside a circular tube [13,21].

Coating paint was produced by combining 1.5 g of Al_2O_3 and TiO_2 particles with 0.4 ml epoxy (Omegabond 200) and 10 ml isopropyl alcohol. Paint was stirred and heated with a magnetic stirrer (Model MS300) and cured at 204 °C for 2 h in a furnace. Apart from improving strength, the heating treatment also helped to form a microporous structure due to evaporation of the highly volatile solvent carrier. Three different sized particles (Aldrich, USA) were used for coating:

(i) Al_2O_3 ($d < 10$ μm)
(ii) TiO_2 ($d < 5$ μm)
(iii) Al_2O_3 ($d < 1$ μm)

The homogeneously mixed slurry was applied inside a circular tube using a spray gun. The tube was rotated until the coating had dried. Scanning electron microscope (SEM) images of surface of microporous Al_2O_3, TiO_2 and nanoporous Al_2O_3 were taken (Figs. 3–5). Microporous $Al_2O_3$and TiO_2 resulted in an ordered porous structure, while nanoporous Al_2O_3 particles agglomerated on the surface. Some cracks were observed on the coated surface after performing the CHF experiments at several conditions, especially in the case of nanoporous coatings. Overall, because of 2 h heat treatment in furnace, the adhesion strength was good enough for microporous coatings and very little aging effects observed.

3.1. Wettability test

The extent to which the liquid phase spreads over the solid phase is called wettability. The wettability of a solid by a liquid is characterized in terms of the angle of contact that the liquid makes on the solid. Porous surface coatings have the capability to entrap water in surface arteries or pores, increasing wettability and decreasing contact angle. Porous coatings are hydrophilic while smooth surfaces are hydrophobic.

The hydrophilicity of coated surfaces was investigated through increase or decrease of contact angle, which is a function of surface roughness. Smooth and coated tubes were weighed dry, soaked in water and re-weighed to check the surface capability of water entrapment and the mass of water entrapped in surface micropores. The liquid was drained by holding the tubes in upright position for 5 min, so that the water remained only in the pores of the coatings. The digital weighing balance Ohaus Scout II was used for recording measurements and the wettability index test was conducted three times to assess the uncertainty. The wettability index results were described on a per unit surface area basis.

A water drop test was performed to check the wettability of coated surfaces. Water dropped on a dry coated surface strip (area = 1 cm^2) showed a high contact angle,

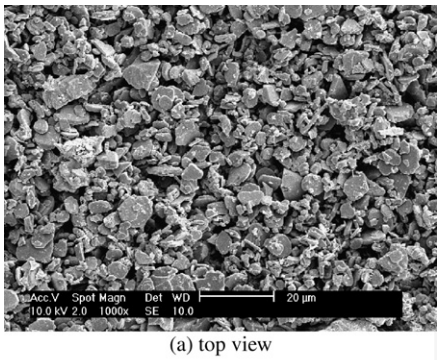

(a) top view

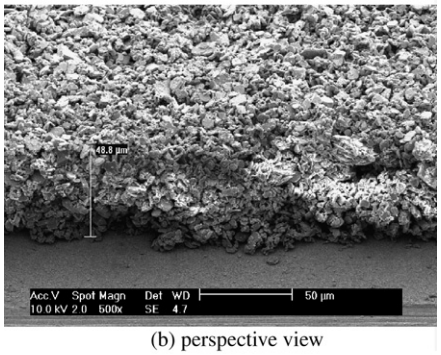

(b) perspective view

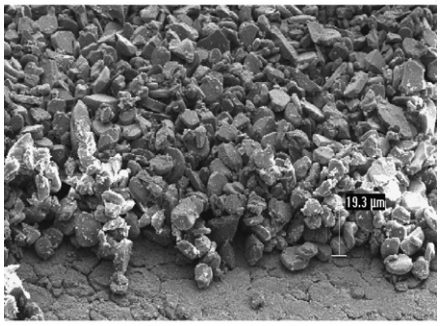

(c) perspective view

Fig. 3. (a) SEM image of coated microporous Al_2O_3 (particle diameter <10 μm); (b) and (c) shows the coating thickness of about 50 and 20 μm, respectively.

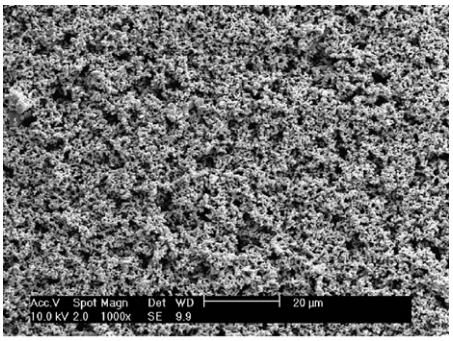

(a) top view

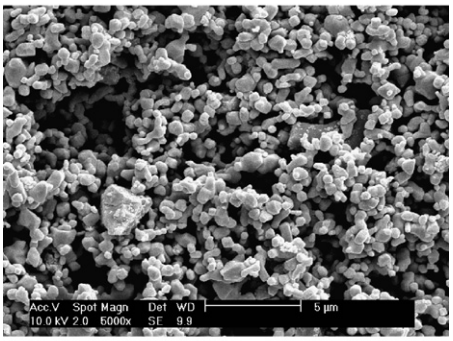

(b) top view

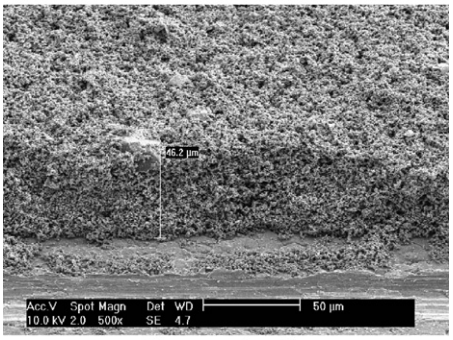

(c) perspective view

Fig. 4. (a) and (b) SEM image of coated microporous TiO_2 (particle diameter <5 μm), with 1000× and 5000× magnifications, respectively; (c) shows the coating thickness of about 50 μm.

meaning decreased wettability and less hydrophilic nature. Water dropped on a wet (water soaked) surface spread out suddenly giving a decreased contact angle, meaning increased hydrophilic nature.

4. Results and discussion

All experiments were performed in flow boiling water at atmospheric pressure in fixed inlet conditions of temperature

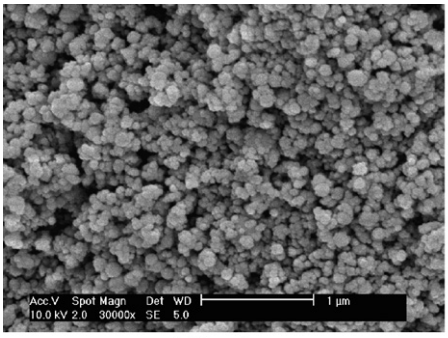

(a) top view

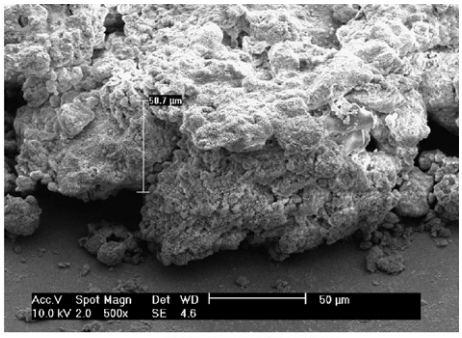

(b) perspective view

Fig. 5. SEM images of coated nanoporous Al_2O_3 particles with a coating thickness of 50 μm; (a) 30,000× magnification, (b) 500× magnification.

and mass flux. The number and size of cavities are related to efficient heterogeneous nucleation and boiling heat transfer enhancement. It is difficult to determine the optimum number, size and shape of cavities on the heated surface. The degree of surface wettability influences how rapidly the cavities are filled with liquid. The formation of bubble at the initiating sites promotes the formation of bubbles on adjacent sites [17].

Boiling heat transfer curves, at inlet subcooling temperatures of 50 °C and 75 °C and at low mass fluxes of 100, 200 and 300 kg/m^2 s for coated tubes compared to the smooth tube are shown in Figs. 7 and 8. Particle size and thickness of coatings are listed in Table 2. A maximum increase in CHF (~25%) was observed with Al_2O_3 microporous tube at an inlet subcooling temperature of 75 °C. Microporous TiO_2 coated tubes also showed a CHF increase of ~20%, as compared to reference smooth tubes. A reduction in wall superheat was observed with Al_2O_3, which was not seen with TiO_2. CHF enhancement comparison of nanoporous Al_2O_3 with the smooth tube was not distinct and prominent, because of agglomeration of nanoparticles, as shown in the SEM image (Fig. 5). This may be due to the coating method [21], which may not be appropriate for nanoporous coatings. The adhesion strength of nanoporous coatings manufactured by this process [21] was weak to sustain the flow boiling experiment.

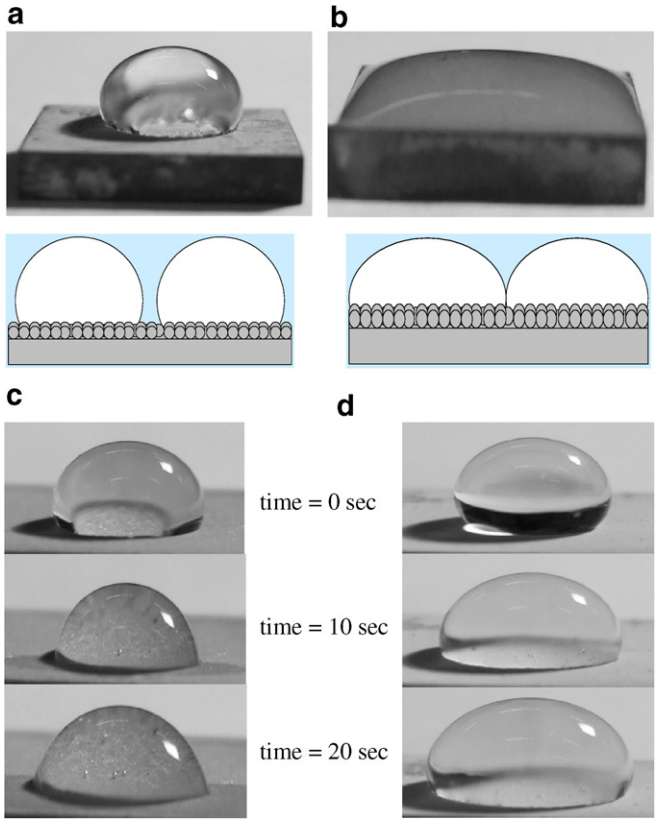

Fig. 6. Shape of water droplets on coated surfaces: (a) and (c) Microporous Al_2O_3 (dry surface), (b) Microporous Al_2O_3 (wet surface), (d) Microporous TiO_2 (dry surface).

The linear trend of CHF as function of mass flux (100–300 kg/m^2 s) is shown at inlet subcooling temperatures of 50 °C and 75 °C (Fig 9). The maximum increase in CHF was observed for microporous Al_2O_3 as compared to microporous TiO_2 and nanoporous Al_2O_3 (Fig. 9a).

A microporous coating thickness optimization study was performed. Coating thickness was measured by cross sectional measurements of SEM images. CHF experiments

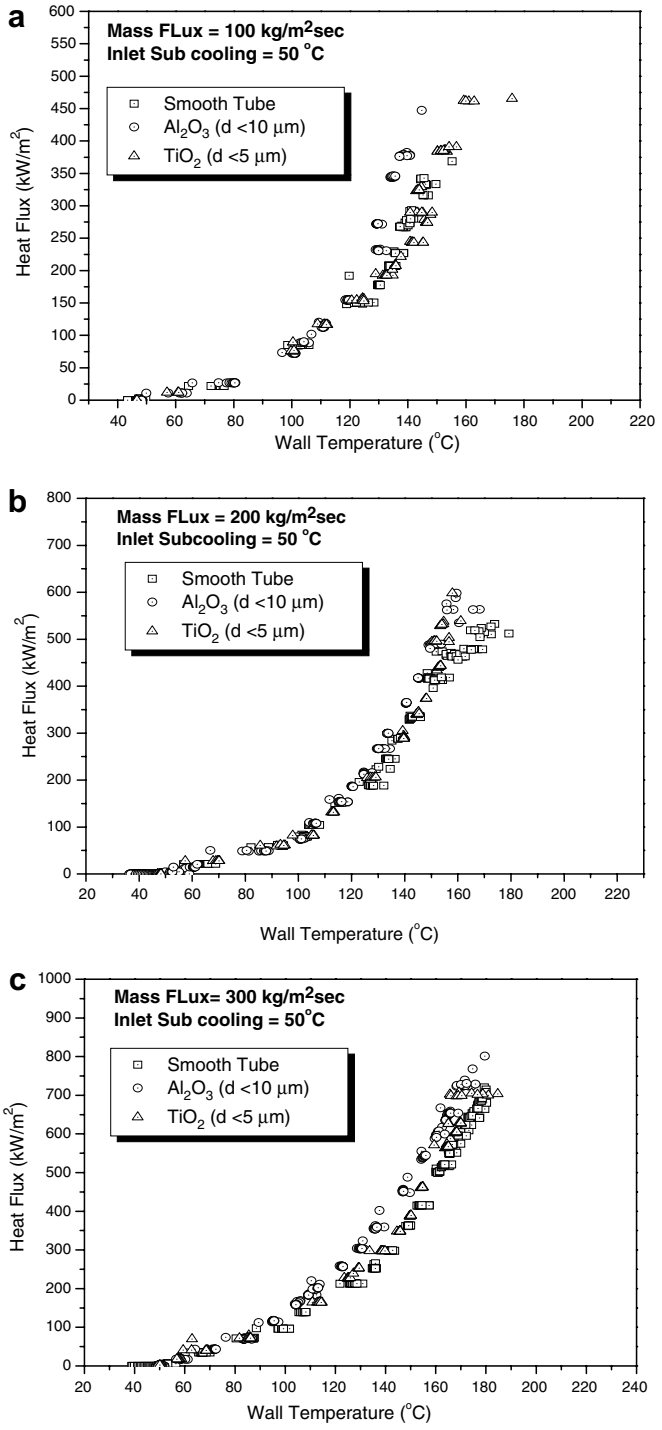

Fig. 7. Boiling curve comparison for coatings at 100 (a), 200 (b) and 300 (c) kg/m^2 s, at inlet subcooling temperature of 50 °C.

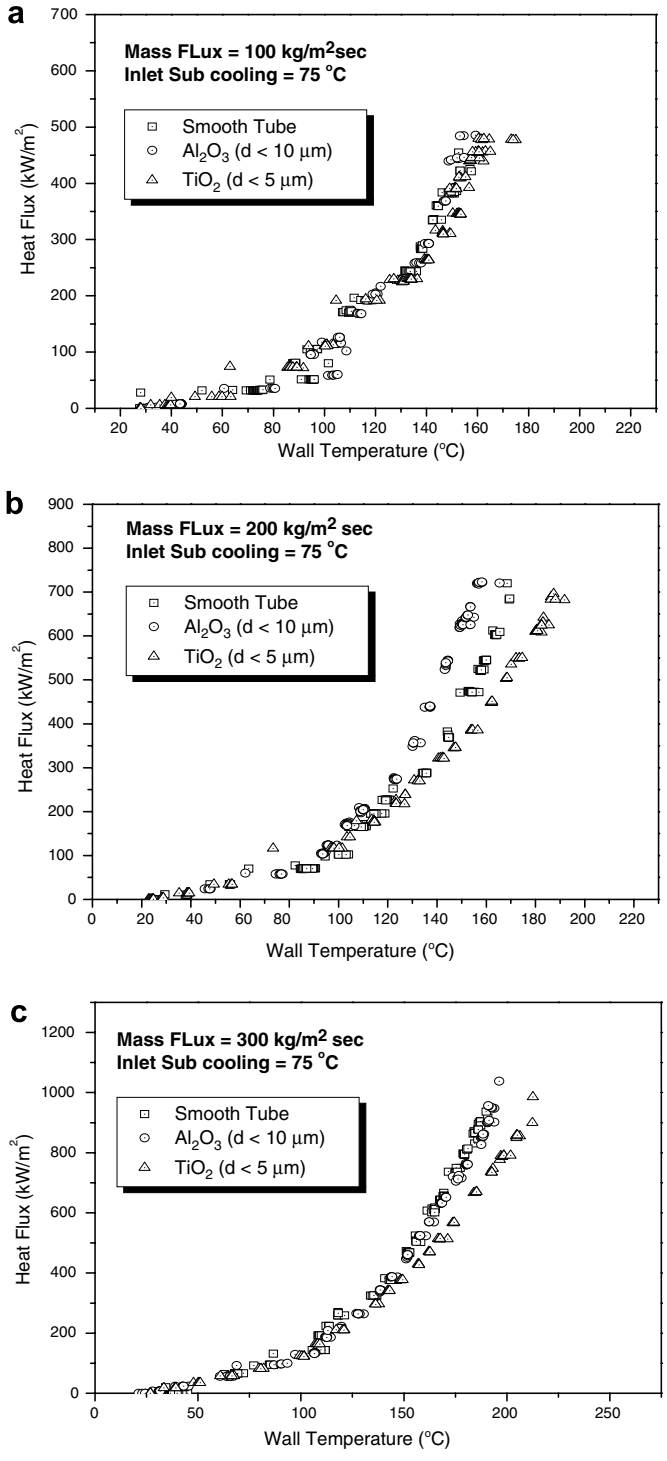

Fig. 8. Boiling curve comparison for coatings at 100 (a), 200 (b) and 300 (c) kg/m^2 s, at an inlet subcooling temperature of 75 °C.

Table 2
Particle sizes and thickness of coatings

No.	Material	Particle size (d)	Coating thickness (t_c)
1	Al_2O_3	<10 μm	~50 μm
2	TiO_2	<5 μm	~50 μm
3	Al_2O_3	<1 μm	~50 μm
4	Al_2O_3	<10 μm	~20 μm

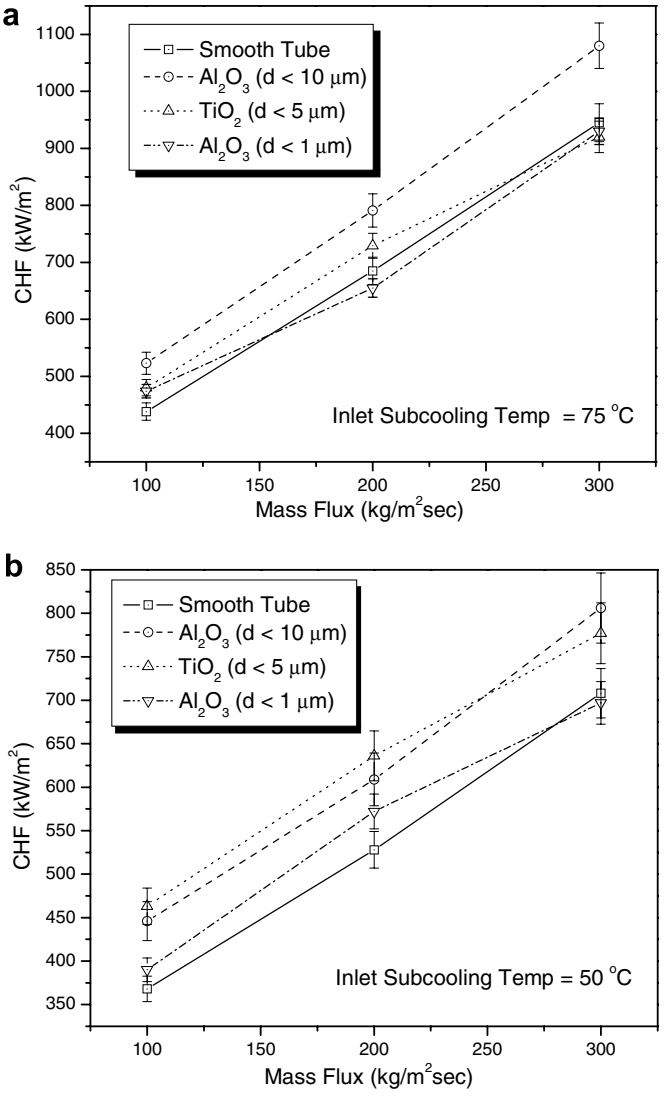

Fig. 9. CHF as a function of mass flux for coating materials at 75 °C (a) and 50 °C (b) inlet subcooling temperatures.

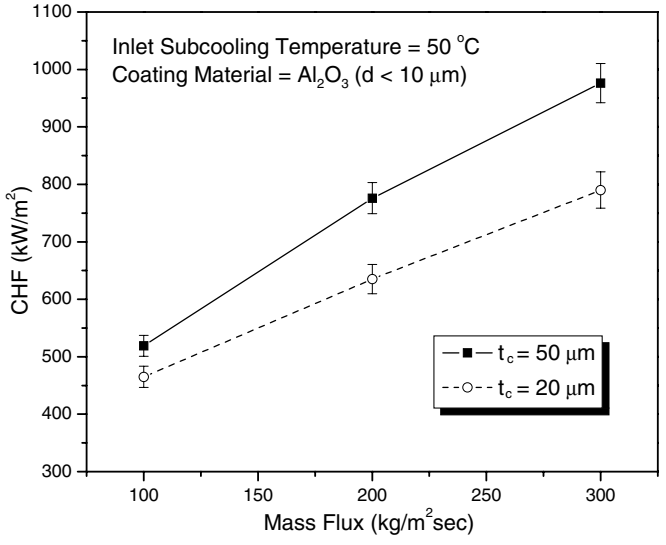

Fig. 10. Effect of mass flux on CHF for Al_2O_3 microporous coatings of 20 μm and 50 μm thickness.

were conducted for two different thickness coatings (20 μm and 50 μm) for microporous Al_2O_3 ($d < 10$ μm). At all mass fluxes (100–300 kg/m^2 s), CHF values were higher for 50 μm thick coated tubes than for 20 μm thickness (Fig. 10). Liter and Kaviany [3] found the same result with the dual-height modulated porous layer coating structure. Chang and You [10] also observed a similar phenomenon with coating thickness in nucleate boiling heat transfer. The porous non-conducting surfaces with layered particle sizes and thicker coatings produced higher heat transfer coefficients (h) at low mass fluxes. The increase of h was thought to be due to increased active nucleation site density for the layered particle sizes within the extended superheated liquid layer. As particle size increased over the microporous coating regime ($0 < d < 20$ μm), the incipient superheat decreases significantly [10].

Wettability index is defined as the measure of weight of entrapped water in micropores per unit surface area of tubes. The wettability index for porous coatings is shown in Table 3. Coatings with micropores retained more water, providing efficient capillary action. A wetted microporous surface decreases the contact angle which is associated with enhanced heat transfer and CHF. The wettability index for Al_2O_3 microporous coated tubes was high as compared to microporous TiO_2 and nanoporous Al_2O_3. Shapes of water droplets on coated dry and wet surfaces are shown in Fig. 6. The high porosity of Al_2O_3 increased wettability. Chang and You [2] found that a reduction in porosity led to lower internal vaporization rates (thin film and capillary vaporization), since there is less liquid within the microstructure to vaporize. Water entrapped inside micropores of wet surface helped to decrease the contact angle and increase wettability. A similar phenomenon happens when water flows through microporous coated tubes increasing CHF as compared to smooth tubes, due to the capillary action of entrapped water in pores. Microporous Al_2O_3 had a smaller contact angle than does TiO_2. During nucleate boiling, prior to CHF, the dry spot region beneath the bubbles requires high wettability to enhance CHF.

Al_2O_3 microporous coatings with a particle size ~10 μm and coating thickness of 50 μm showed increased CHF as compared to microporous TiO_2 and nanoporous Al_2O_3 coatings. Although the thermal conductivity of Al_2O_3 was high ($k = 25$ W/m K) as compared to TiO_2 ($k = 6.69$ W/m K), it was not the major factor observed for CHF enhancement, since the enhancement performance of TiO_2 was better than nanoporous Al_2O_3. Microporous coatings provide improved nucleation site densities, helping to entrap more water volume.

Table 3
Wettability index of coatings

Coating material ($t_c = 50$ μm)	Al_2O_3 ($d < 10$μm)	TiO_2 ($d < 5$μm)	Al_2O_3 ($d < 1$ μm)
Bare weight per surface area of coated tube, W1 (kg/m^2)	12.556	12.545	12.523
Wet weight per surface area of coated tube, W2 (kg/m^2)	12.618	12.595	12.560
Wettability index, W2–W1 (kg/m^2)	0.062	0.050	0.037

5. Conclusions

Subcooled water flow boiling CHF using micro/nanoporous surface coatings inside SS316 tubes at atmospheric pressure was studied. Significant findings were:

(1) Enhanced (~25%) CHF was observed for microporous Al_2O_3 coated surface as compared to smooth tube. Microporous TiO_2 coated surface showed ~20% enhancement as compared to smooth tube. CHF enhancement was insignificant in nanoporous Al_2O_3 coated tube, due to the agglomeration of nanoparticles. Nanoporous coatings, produced by opted method [21], did not have sufficient adhesion strength to sustain the flow boiling experiment. Microporous coatings proved better for flow boiling CHF enhancement as compared to nanoporous coatings.
(2) Microporous Al_2O_3 had a high wettability index, with greater entrapment of water in pores. Enhancement of CHF due to increased particle size can be explained by increased nucleation sites. Microporous Al_2O_3 had better heat transfer enhancement than TiO_2, while nanoporous Al_2O_3 showed less CHF enhancement than TiO_2.
(3) Larger sized micro-particle coatings produced more nucleation sites and resulted in pores with better water entrapment capabilities, optimizing heat transfer enhancement. Particle sizes of 5–10 μm and coating thickness of about 50 μm were most effective for CHF enhancement.
(4) CHF enhancement is greater at inlet subcooling temperature of 75 °C than at 50 °C. Thus, CHF enhancement of microporous coated surfaces increases with increased subcooling. Critical heat flux varied proportionately as a function of mass flux. CHF enhancement at a mass flux of 300 kg/m^2 s was greater than at 100 kg/m^2 s.

Acknowledgements

The authors would like to express their gratitude to Dr. In Cheol Bang of KAIST (presently working as post-doc at MIT, USA) for his great help.

References

[1] S.G. Kandlikar, Critical heat flux in subcooled flow boiling – an assessment of current understanding and future directions for research, Multiphase Sci. Technol. 13 (32) (2001) 207–232.
[2] J.Y. Chang, S.M. You, Enhanced boiling heat transfer from microporous surfaces: effects of a coating composition and method, Int. J. Heat Mass Transfer 40 (18) (1997) 4449–4466.
[3] Scott G. Litter, M. Kaviany, Pool-boiling CHF enhancement by modulated porous layer coating: theory and experiment, Int. J. Heat Mass Transfer 44 (18) (2001) 4287–4311.

[4] M. Kaviany, Principles of Heat Transfer in Porous Media, second ed., Springer, New York, 1995, pp. 20–21.
[5] L.S. Tong, Y.S. Tang, Boiling Heat Transfer and Two-Phase Flow, second ed., Taylor & Francis, USA, 1997, pp. 391–398.
[6] Srinivas Vemuri, K.J. Kim, Pool boiling of saturated FC-72 on nanoporous surfaces, Int. Commun. Heat Mass Transfer 32 (1–2) (2005) 27–31.
[7] D. Schroeder-Richter, S. Yildiz, G. Bartsch, Effect of porous coating on critical heat flux, Int. Commun. Heat Mass Transfer 23 (4) (1996) 463–471.
[8] Tomoaki Kunugia et al., Ultrahigh heat transfer enhancement using nanoporous layer, Superlattices Microstruct. 35 (2004) 531–542.
[9] C.N. Ammerman, S.M. You, Enhancing small-channel convective boiling performance using a microporous surface coating, Trans. ASME 123 (2001) 976–1083.
[10] J.Y. Chang, S.M. You, Boiling heat transfer phenomena from microporous and porous surfaces in saturated FC-72, Int. J. Heat Mass Transfer 40 (18) (1997) 4437–4447.
[11] K.N. Rainey, G. Li, S.M. You, Flow boiling heat transfer from plain and micro-porous coated surfaces in subcooled FC-72, Trans. ASME 123 (2001) 918–925.
[12] Janusz T. Cieslinski, Nucleate pool boiling on porous metallic coatings, Exp. Thermal Fluid Sci. 25 (2002) 557–564.
[13] J.P. O'Connor, S.M. You, A painting technique to enhance pool boiling heat transfer in saturated FC-72, ASME J. Heat Transfer 117 (2) (2001) 387–393.
[14] K. Ferjancic Golobic, The role of enhanced coated surface in pool boiling CHF in FC-72, Heat Mass Transfer 36 (2000) 525–531.
[15] Shou-Shing Hsieh et al., Nucleate pool boiling characteristics from coated tube bundles in saturated R-134a, Int. J. Heat Mass Transfer 46 (2003) 1223–1239.
[16] J.H. Kim, S.M. You, Stephen U.S. Choi, Evaporative spray cooling of plain and microporous coated surfaces, Int. J. Heat Mass Transfer 47 (2004) 3307–3315.
[17] Vijay K. Dhir, Mechanistic prediction of nucleate boiling heat transfer – achievable or a hopeless task? J. Heat Transfer 128 (2006).
[18] Robert J. Moffat, Describing the uncertainties in experimental results, Exp. Thermal Fluid Sci. 1 (1988) 3–17.
[19] F.B. Cheung, Limiting factors for External Reactor Vessel Cooling, NURETH-10, Seoul, Korea, October 5–9, 2003.
[20] J. Yang, B. Dizon, F.B. Cheung, K.Y. Suh, S.B. Kim, CHF enhancement by vessel coating for external reactor vessel cooling, in: Proceedings of ICAPP '04, Pittsburgh, USA, June 13–17, 2004.
[21] J.P. O'Connor, S.M. You, Boiling enhancement coating, U.S. Patent No. 5814392, 1998.